Filtering of measurement noise with the 3D reconstruction algorithm

Cappellin, Cecilia; Pivnenko, Sergey

Published in:
Proceedings of the 36th Annual Symposium of the Antenna Measurement Techniques Association (AMTA)

Publication date:
2014

Filtering of Measurement Noise with the 3D Reconstruction Algorithm

C. Cappellin[1], S. Pivnenko[2]
[1]TICRA, Læderstræde 34, DK-1201 Copenhagen, Denmark
[2]DTU Elektro, Technical University of Denmark, Ørsteds Plads, Building 348, 2800 Kgs. Lyngby, Denmark

Abstract— **Two different antenna models are set up in GRASP and CHAMP, and noise is added to the radiated field. The noisy field is then given as input to the 3D reconstruction of DIATOOL and the SWE coefficients and the far-field radiated by the reconstructed currents are compared with the noise-free results coming from GRASP and CHAMP. The obtained results are presented and discussed.**

I. INTRODUCTION

The 3D reconstruction algorithm of DIATOOL, with its higher-order Method of Moments-based implementation, reconstructs extreme near fields and surface currents on arbitrary 3D surfaces enclosing the antenna under test (AUT) from the measured radiated field. DIATOOL is a valuable analysis and diagnostics tool for the antenna engineer to speed up the antenna prototyping cycle and identify errors in the manufactured AUTs, since the 3D reconstruction can solve a number of problems which traditional microwave holography cannot handle, namely:

1. Accurate and detailed identification of array malfunctioning due to the enhanced spatial resolution of the reconstructed fields and currents
2. Filtering of the scattering from support structures and feed network leakage

A number of papers published over the past four years have shown these features in detail [1-4]. At the same time it was observed that the spherical wave expansion (SWE) of the field radiated by the currents reconstructed by DIATOOL always provides a power spectrum that looks noise-free. This phenomenon was observed for all the antennas on which the 3D reconstruction was applied, see for example [3]-[4], and it was explained as being an effect of the 3D reconstruction algorithm, which uses the a-priori information that all sources are contained inside the reconstruction surface. However, since real measured data were always used as input, it was not possible to know if the power spectrum of the reconstructed currents coincided with the one coming from noise-free measurements.

The purpose of the present paper is thus to investigate in detail the noise filtering capabilities of the 3D reconstruction algorithm of DIATOOL.

Two different antenna models were set up in GRASP and CHAMP and noise was added to the radiated field. The noisy field was then given as input to DIATOOL, and the SWE coefficients and the far-field radiated by the reconstructed currents were compared with the noise-free results coming from GRASP and CHAMP.

The paper is organized as follows: in Section II the 3D reconstruction of DIATOOL is briefly summarized. In Section III, the reconstruction is applied to the GRASP model of the prototype feed array of the BIOMASS synthetic aperture radar, while in Section IV the same is repeated for an axially corrugated horn modelled in CHAMP. Conclusions are finally drawn in Section V.

II. THE 3D RECONSTRUCTION OF DIATOOL

DIATOOL computes the equivalent electric and magnetic surface current densities $\bar{J}s$ and $\bar{M}s$ on a reconstruction surface *S* enclosing the AUT, from the field measured at discrete points outside the surface. These equivalent currents correspond to Love's equivalence principle, since they produce zero field inside *S*. They are related to the measured data through the so-called data equation,

$$\bar{E}^{meas} = -\eta_0 L\bar{J}s + K\bar{M}s, \qquad (1)$$

where η_0 is the free space impedance and L and K are the integral operators defined in [5]. The a priori information that the fields radiated by the surface current densities must be zero inside *S* is used and enforced as a boundary condition equation [5]. The surface of reconstruction is discretized using curvilinear patches of up to fourth order. The electric and magnetic surface currents densities on each patch are expanded in higher order Legendre basis functions [5]. The current expansion is then inserted in the data equation of Eq. (1) and the above mentioned boundary condition equation. These coupled equations constitute an inverse problem, and are therefore solved with a special regularization scheme [5] which allows one to achieve an accurate solution by balancing the effects of the noise with the requirement of achieving Love's currents, since the data equation and the boundary condition are treated separately. This results in improved efficiency, enhanced accuracy, and better resolution properties. The reconstructed equivalent currents are later used in a direct linear integral equation in order to find their radiated field. The field radiated by the equivalent currents is very similar to the measured field, and it coincides with it if the measured field is not affected by noise.

III. THE PROTOTYPE FEED ARRAY OF THE BIOMASS SYNTHETIC APERTURE RADAR

The first example used in this paper is the prototype feed array of the large deployable reflector of the BIOMASS mission. The feed array is a 2×2 patch array of about 1 m^2 located on a rectangular ground plane, and working at 435 MHz. The feed array was measured at the DTU-ESA Spherical Near-Field Antenna Test Facility, by using a rectangular support structure of aluminum to mount the feed array antenna on the antenna positioner, see Figure 1. Spherical near-field measurements showed a too large effect of the metallic support frame. In [2] it was shown how DIATOOL could be used to filter the contribution of the support structure and its coupling with the unwanted radiation of the array feeding network.

In the present paper, the GRASP model developed in [2] is used. It consists of the four patches, the ground plane and the metallic support frame. Four *x*- and *y*-oriented magnetic dipoles, properly excited and located just behind the patch array, are also added in order to model the unwanted radiation of the array feeding network. Method of Moments (MoM) is used to compute the radiated field. This field will be called in the following reference field. A Gaussian white noise with SNR equal to 60 dB is then added to the reference field, in order to simulate the measurements performed at the DTU-ESA facility. This field will be called in the following noisy field.

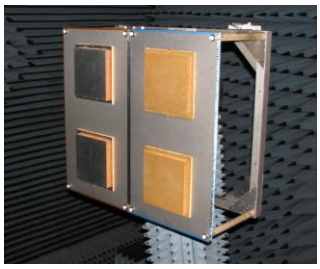

Figure 1 The prototype feed array and its test support frame on the measurement tower.

The noisy field is computed on a full sphere with sampling in theta and phi of 5 deg, and used as input to DIATOOL. The equivalent currents are reconstructed on a closed box conformal to the feed array and the support frame, located 400 mm behind the array, as shown in Figure 2.

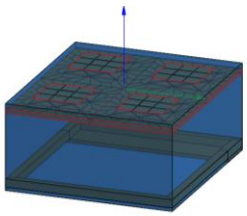

Figure 2 DIATOOL reconstruction surface shown in blue: the surface encloses the feed array and the support frame.

The Spherical Wave Expansion (SWE) of the far-field radiated by the reconstructed equivalent currents as well as the far-field on the phi=0 and 90 deg planes are also computed by DIATOOL. We will refer in the following to these quantities as filtered SWE and filtered field, respectively. A plot of the SWE power spectra is shown in Figure 3, where kr_o for the antenna is equal to 5.

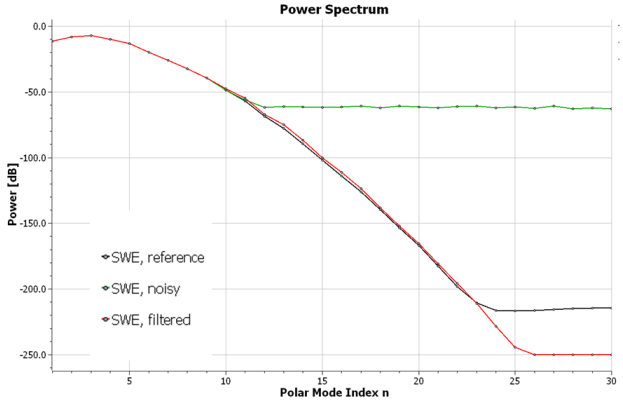

Figure 3 Power spectra for the feed array and the support frame: in green the noisy one with 60 dB noise, in black the reference one, and in red the filtered one.

It is seen that the noisy power spectrum (green curve) presents a noise floor of around -60 dB, by which only the first 11 modes can be trusted. The reference spectrum (black curve) and the filtered spectrum (red curve) reach a noise floor located below -200 dB. It is also seen, as expected, that the three spectra coincide for *n* smaller than 9. By zooming Figure 3, it is observed that the black and red curves follow the same envelope, but that the values for a certain *n* do not exactly coincide, like for *n* smaller than 9. The difference is about 2 dB for *n* up to 18, and around 1.5 dB for *n* larger than 18. Since the filtered power spectrum of Figure 3 is slightly above the reference spectrum, the equivalent currents located on the reconstruction surface are electrically slightly larger than the currents considered by GRASP.

It is now interesting to see how the field radiated by the equivalent currents computed by DIATOOL, i.e. the filtered field, looks like. In Figure 4 the amplitude of the reference far-field, the noisy far-field and the filtered far-field are compared, for phi=0, together with their complex differences. The continuous curves show the effect of the noise over the reference field, and show the typical spikes of a Gaussian noise distribution. The dashed lines show the difference between the reference field and the filtered field computed by DIATOOL. It is seen that Gaussian spikes have disappeared. For the phi component, the filtered field is closer to the reference field, while for the theta component the noisy field is closer to the reference field. The differences on phi=90 are similar to the one shown in Figure 4, except for the fact that the theta and phi components are interchanged, as the reference field does.

It is then decided to compare the far-fields obtained from the SWE. In Figure 5 all coefficients contained in the SWE of Figure 3 are used, while in Figure 6 a truncation in *n* equal to *N*=11, i.e. before the noise floor, is applied. It is seen that the

differences between the reference and the filtered field (dashed curves) are the same in Figure 4, Figure 5 and Figure 6.

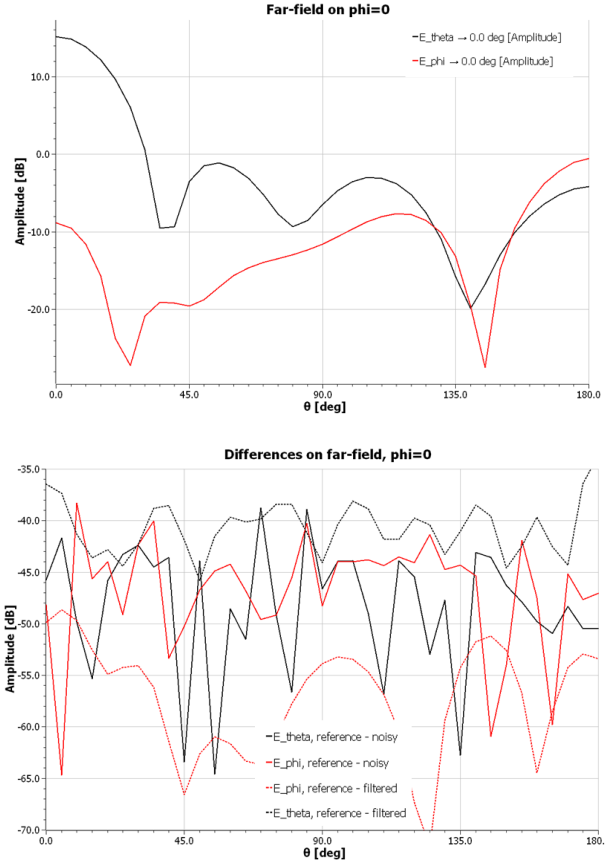

Figure 4 Far-field patterns for phi=0 and their difference.

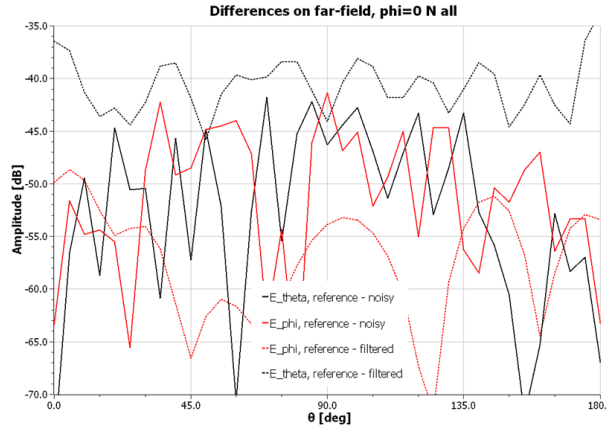

Figure 5 Far-field differences from SWE (*n*=all) for phi=0.

The differences between the reference and the noisy field are the same in Figure 4 and Figure 5 except for a difference in the first ten degrees, but clearly decrease in amplitude in Figure 6 showing also a smoother envelope. It was also seen that the differences between the reference far-field obtained with *N*=11 and the one obtained with *N*=30 were negligible and around -65 dB. The same happened for the filtered field, while the differences for the noisy field were around -45 dB. This means that the additional modes between 12 and 30 of the SWE depicted in Figure 3 do not significantly contribute to the reference and filtered field, since their amplitude is too low. With this in mind, and by comparing Figure 6 with Figure 5 for the difference between the reference and the noisy field, we can conclude that it is advisable to truncated the SWE to *N*=11, i.e. before the noise floor. By doing that, the noisy field becomes closer than the filtered field to the reference field. The same behaviour of Figure 4 - Figure 6 was observed by plotting the field differences on a sphere of radius 1 m. The experiment was then repeated by considering a 40 dB SNR noisy field. The same observations of Figure 4 - Figure 6 could be made.

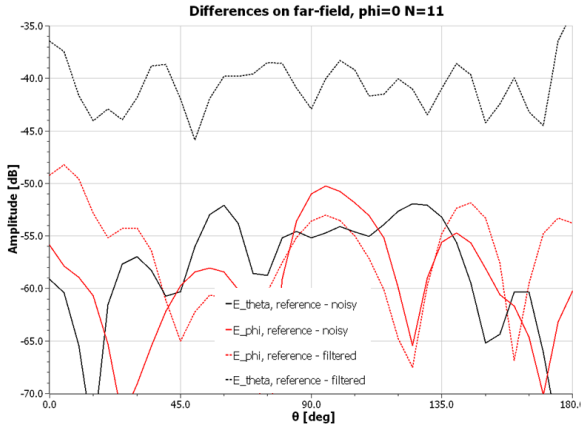

Figure 6 Far-field differences from SWE (*N*=11) for phi=0.

From Figure 6 we can deduce that the SWE coefficients up to *N*=11 do not coincide with each other for the noisy, reference and filtered case. In particular, it seems that the coefficients of the filtered field deviate from the reference field more than what the noisy field does. It was thus decided to look more in detail into the values of the SWE coefficients. In Figure 7 a plot of the amplitude and phase of Q_{10n} and Q_{20n} is given.

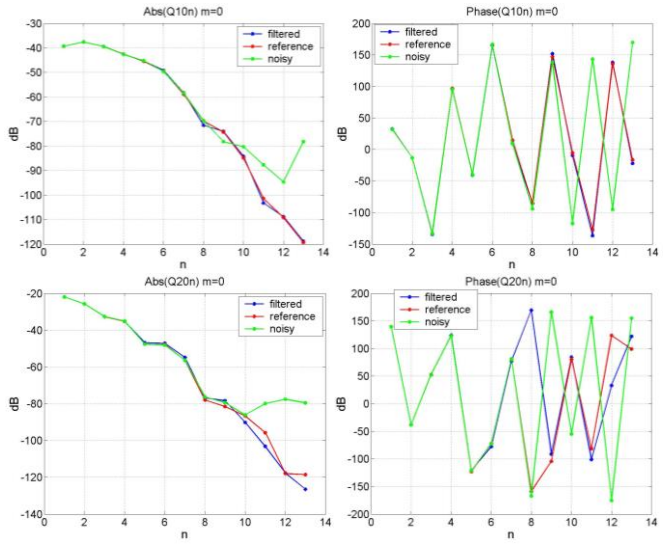

Figure 7 Amplitude and phase of Q_{10n} (above) and Q_{20n} (below): in green noisy, in red filtered and blue reference.

It is possible to see that up to n=6 the values coincide. For $7 \leq n \leq 11$ differences in amplitude and/or phase start appearing: the amplitudes of the filtered Q_{10n} and Q_{20n} (blue curve) differ from the one of the noisy and reference. The phases seem in better agreement, except a significant difference of Q_{20n} for n=10. A similar variation can be expected for the other modes. Finally, the amplitude of the equivalent currents reconstructed by the 3D reconstruction from the noisy field is shown in Figure 8 together with the currents reconstructed from the noise-free reference field. The four patches are visible and the pictures are in very good agreement. The result given by traditional microwave holography of the noisy field is shown in Figure 9. It is seen that the four patches cannot be resolved.

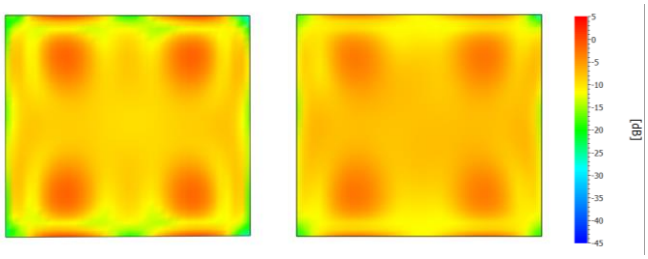

Figure 8 Amplitude of the total electric currents reconstructed on the top face of the reconstruction surface of Figure 2: to the left from the reference field, to the right from the noisy field.

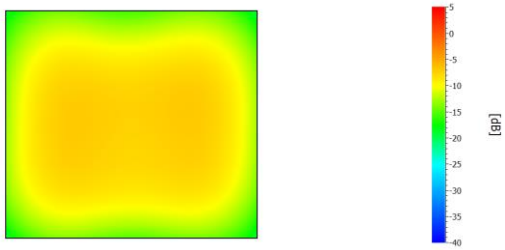

Figure 9 Amplitude of the total electric currents reconstructed on the top face of the reconstruction surface of Figure 2 with microwave holography of the noisy field.

IV. AXIALLY CORRUGATED HORN

The second example of this paper is a linearly polarized axially corrugated horn modelled by CHAMP, working at 8 GHz, and with an aperture of two wavelengths. The reference field was computed by CHAMP, and a white Gaussian noise of SNR of 40 dB was added to it. The noisy field was given as input to DIATOOL and the equivalent currents were reconstructed by the 3D reconstruction algorithm on a closed surface conformal to the antenna, as depicted in Figure 10. The Spherical Wave Expansion (SWE) of the far-field radiated by the reconstructed equivalent currents as well as the far-field on the phi=0, and 90 deg planes were also computed by DIATOOL. A plot of the power spectra is shown in Figure 11, where kr_o for the antenna is equal to 6. The noisy power spectrum (green curve) presents a noise floor of around -60 dB, by which only the first 10 modes can be trusted. The reference spectrum (black curve) and the filtered spectrum (red curve) reach a noise floor at -250 dB, but the curves do not coincide.

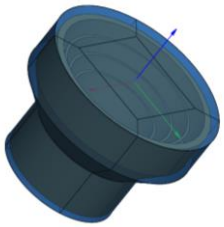

Figure 10 Axially corrugated horn enclosed by the reconstruction surface defined by DIATOOL.

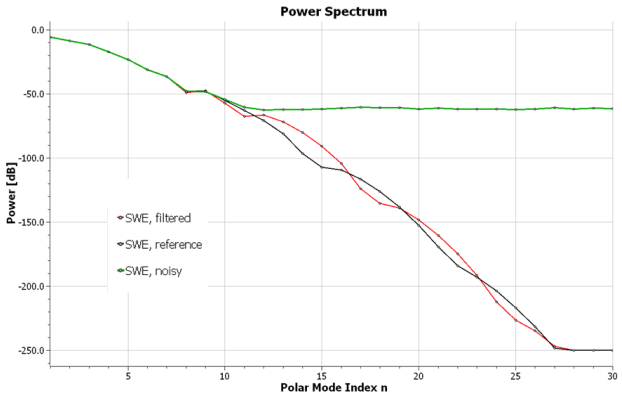

Figure 11 Power spectra for the horn: in green the noisy one, in black the reference one, and in red the filtered one.

In Figure 12 the amplitude of the complex differences between the reference far-field, the noisy far-field and the filtered far-field are compared for phi=0.

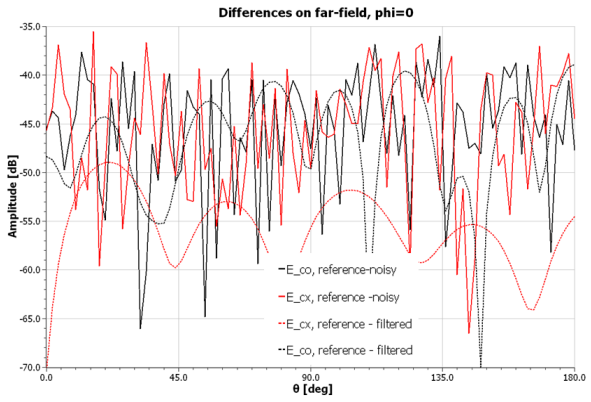

Figure 12 Far-field patterns for phi=0 and their difference.

The continuous curves represent the effect of the noise over the reference field, and show the typical spikes of a Gaussian

noise distribution. The dashed lines show the difference between the reference field and the filtered field computed by DIATOOL. It is seen that the Gaussian spikes have disappeared and that the dashed curves are lower than the continuous lines

The far-fields obtained from the SWE are then compared: in Figure 13 all coefficients contained in the SWE of Figure 11 are used, while in Figure 14 a truncation in n equal to N=10, i.e. before the noise floor, is used.

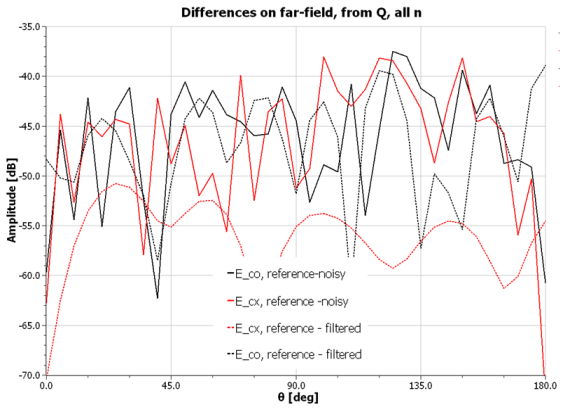

Figure 13 Far-field differences from SWE (n=all) for phi=0.

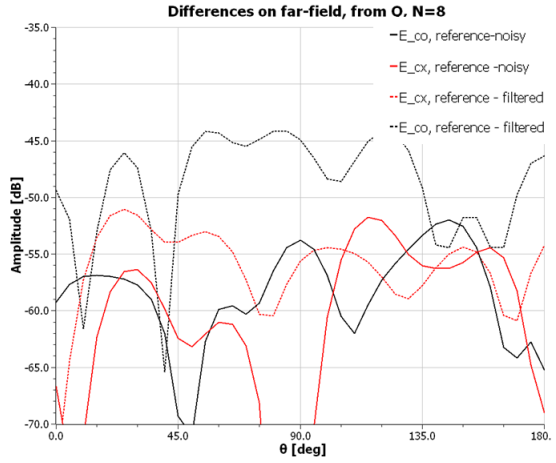

Figure 14 Far-field differences from SWE (N=10) for phi=0.

Figure 13 agrees with Figure 12, i.e. the filtered field is closer than the noisy field to the reference field. Figure 14 shows again, like Figure 6, that the noisy field gets closer than the filtered field to the reference field when the modes are truncated. A plot of the amplitude and phase of the Q_{1mn} and Q_{2mn} modes for m=1 is finally given in Figure 15. The amplitude and phases of the coefficients seem to coincide up to n=8, while from n=9 the amplitude and/or phase of the filtered modes start disagreeing from the reference. After n=12 the noisy modes clearly disagree as well.

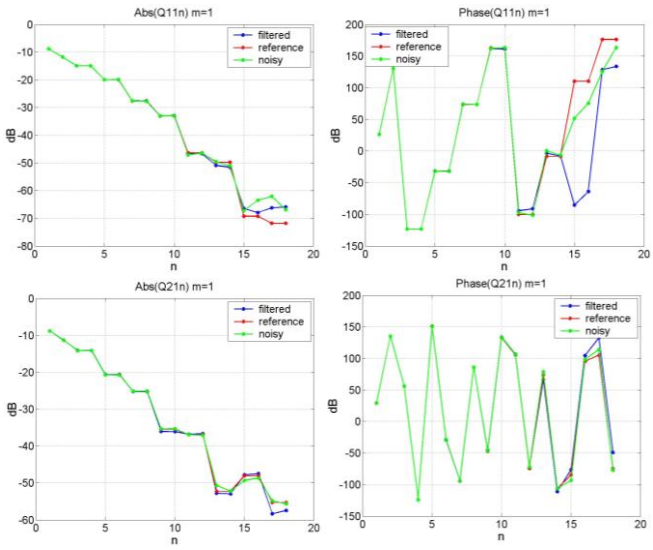

Figure 15 Amplitude and phase of Q_{11n} (above) and Q_{21n} (below): in green noisy, in red filtered and blue reference.

V. CONCLUSIONS

Two different antenna models were set up in GRASP and CHAMP and noise was added to their radiated fields. The noisy field was given as input to DIATOOL, and the SWE coefficients and the far-field radiated by the reconstructed currents, denoted filtered SWE and filtered field respectively, were computed. These were compared with the noisy data and the reference data coming from GRASP and CHAMP.

The first antenna was the feed array of the BIOMASS mission, with a SNR was equal to 60 dB, while the second antenna was an axially corrugated horn with a SNR of 40 dB. For both antennas, the filtered power spectrum looked like a noise-free version of the noisy input field. The power spectrum of the filtered and reference fields showed a noise floor of around -200 dB, while the power spectrum of the noisy field had a noise floor of around -60 dB. In spite of the similar low noise floor, the filtered power spectrum did however not fully coincide with the reference power spectrum, for both antennas. This could be seen directly from the power spectra plots and was investigated more in details for a series of spherical Q coefficients. The difference between the reference and the filtered field had a smooth pattern, while the difference of the reference and the noisy field showed the typical spikes of a noisy field. For the feed prototype, the filtered field was closer than the noisy field to the reference field, but only for one component of the field at each phi cut. For the axially corrugated horn, the filtered field was always closer than the noisy field to the reference field, in both components. It was finally observed that truncating the SWE of the noisy field to the last n not affected by the noise floor, provided a very good approximation of the reference field. This approximation was better than the field provided by the filtered field.

REFERENCES

[1] C. Cappellin, P. Meincke, S. Pivnenko, E. Jørgensen, "Array antenna diagnostics with the 3D reconstruction algorithm", Proc. AMTA 2012.

[2] C. Cappellin, S. Pivnenko, K. Pontoppidan, "Detailed diagnostics of the BIOMASS feed array prototype", Proc. AMTA 2013.

[3] C. Cappellin, S. Pivnenko, E. Jørgensen, P. Meincke, "Array diagnostics, spatial resolution and filtering of undesired radiation with the 3D reconstruction algorithm", Proc. ESA workshop 2013.

[4] C. Cappellin, S. Pivnenko, "Field reconstruction and estimation of the antenna support structure effect on the measurement uncertainty of the BTS1940 antenna ", Proc. EuCAP 2014.

[5] E. Jørgensen, P. Meincke, O. Borries, and M. Sabbadini, "Processing of measured fields using advanced inverse method of moments algorithm", Proc. of the 33rd ESA Antenna Workshop, ESTEC, Noordwijk, The Netherlands, 2011.